Arylsulfatase G inactivation causes loss of heparan sulfate 3-*O*-sulfatase activity and mucopolysaccharidosis in mice

Björn Kowalewski[a], William C. Lamanna[b,1], Roger Lawrence[b,1], Markus Damme[a,1], Stijn Stroobants[c], Michael Padva[d], Ina Kalus[a], Marc-André Frese[a], Torben Lübke[a], Renate Lüllmann-Rauch[e], Rudi D'Hooge[c], Jeffrey D. Esko[b], and Thomas Dierks[a,2]

[a]Biochemistry I, Department of Chemistry, Bielefeld University, 33615 Bielefeld, Germany; [b]Department of Cellular and Molecular Medicine, Glycobiology Research and Training Center, University of California at San Diego, La Jolla, CA 92093; [c]Laboratory of Biological Psychology, Department of Psychology, University of Leuven, 3000 Leuven, Belgium; [d]Biochemistry II, Georg-August University Göttingen, 37073 Göttingen, Germany; and [e]Department of Anatomy, Christian-Albrechts-University Kiel, 24098 Kiel, Germany

Edited by Stuart A. Kornfeld, Washington University School of Medicine, St. Louis, MO, and approved May 7, 2012 (received for review February 6, 2012)

Deficiency of glycosaminoglycan (GAG) degradation causes a subclass of lysosomal storage disorders called mucopolysaccharidoses (MPSs), many of which present with severe neuropathology. Critical steps in the degradation of the GAG heparan sulfate remain enigmatic. Here we show that the lysosomal arylsulfatase G (ARSG) is the long-sought glucosamine-3-*O*-sulfatase required to complete the degradation of heparan sulfate. *Arsg*-deficient mice accumulate heparan sulfate in visceral organs and the central nervous system and develop neuronal cell death and behavioral deficits. This accumulated heparan sulfate exhibits unique nonreducing end structures with terminal *N*-sulfoglucosamine-3-*O*-sulfate residues, allowing diagnosis of the disorder. Recombinant human ARSG is able to cleave 3-*O*-sulfate groups from these residues as well as from an authentic 3-*O*-sulfated *N*-sulfoglucosamine standard. Our results demonstrate the key role of ARSG in heparan sulfate degradation and strongly suggest that ARSG deficiency represents a unique, as yet unknown form of MPS, which we term MPS IIIE.

lysosomes | sulfatases | Sanfilippo syndrome | mouse model

Lysosomal storage disorders (LSDs) comprise a group of inherited metabolic diseases characterized by the accumulation of storage material reflecting a defect of a lysosomal hydrolase or associated protein (1). Deficiencies in six lysosomal sulfatases lead to severe LSDs caused by accumulation of the corresponding sulfated substrate in the lysosome, resulting in the impairment of lysosomal function as well as the initiation of pathological cascades outside the lysosomes (1–3). Arylsulfatase A (ARSA) cleaves sulfated galactosylceramides (4), which, when absent, leads to metachromatic leukodystrophy (5), whereas the other five characterized lysosomal sulfatases [arylsulfatase B, galactosamine-6-sulfatase, (*N*-acetyl)glucosamine-6-sulfatase, heparan-*N*-sulfatase (sulfamidase), and iduronate-2-sulfatase] function in the successive degradation of sulfated glycosaminoglycans (GAGs), namely heparan sulfate, chondroitin sulfate, dermatan sulfate, and keratan sulfate (3). The lysosomal degradation of GAGs occurs stepwise beginning at the nonreducing end (NRE) of the sugar chain. Genetic deficiency of any of the enzymes involved leads to mucopolysaccharidoses (MPSs), a disease group comprising 11 disorders with distinct molecular defects (6).

Among the degradation routes for the different GAGs, heparan sulfate catabolism is the most complex, involving three glycosidases, three known sulfatases, and one acetyltransferase (6). Impairment of any of these enzymes has been linked to a specific form of MPS (MPS I, II, IIIA–D, and VII), all associated with severe neuropathology in affected patients because of massive storage of heparan sulfate (and also secondary metabolites) in the CNS (6). However, the enzymatic removal of two low-abundance sulfate groups, namely 2-*O*-sulfate from glucuronic acid and 3-*O*-sulfate from glucosamine, have remained enigmatic (7, 8), and disorders in which the removal of these sulfate groups is defective have not been reported.

Arylsulfatase G (ARSG), a recently characterized lysosomal sulfatase with unknown physiological substrates (9), has been reported previously to be associated with an adult form of ceroid lipofuscinosis in dogs (10). In this study, we generated an ARSG-deficient mouse model by targeted disruption of the *Arsg* gene. In addition to heparan sulfate storage, we observed pathological changes common to MPS-type LSDs and identified the physiological substrate of ARSG as the *N*-sulfoglucosamine-3-*O*-sulfate moiety of heparan sulfate. Our findings clearly demonstrate that ARSG is the long-sought glucosamine-3-sulfatase and that its deficiency results in a unique type of MPS, which we propose to designate as MPS IIIE (Sanfilippo E).

Results

ARSG-Deficient Mice Show Lysosomal Storage and Cellular Alterations in the CNS. To determine the physiological function of ARSG, we inactivated the gene in mice by insertion of a neomycin-resistance cassette into exon 2 (Fig. S1*A*). *Arsg* inactivation was confirmed by Southern blot analysis, genomic PCR, and RT-PCR (Fig. S1 *B–D*). *Arsg*-knockout mice exhibited normal development, showed no obvious changes in appearance, and were fertile. Macroscopic inspection of organs was unremarkable. In the CNS, no apparent atrophy was evident up to the age of 12 mo; however, several neuronal and microglia populations revealed obvious vacuoles with prominent lysosomal storage pathology in Purkinje cells of the cerebellum and also in perivascular and meningeal macrophages (Fig. 1 *A* and *B* and Fig. S2 *A* and *B*). Thalamic and hippocampal neurons revealed sporadic lysosomal inclusions (Fig. S2 *C* and *D*). Storage vacuoles showed positive periodic acid–Schiff staining (Fig. 1*C*) and appeared partially empty after Epon embedding, indicating water-soluble carbohydrate storage material. Transmission electron microscopy (TEM) of the storage material in Purkinje cells showed lamellar to finely granular structures (Fig. 1*D*). In older animals, storage material revealed autofluorescent properties at different excitation wavelengths (Fig. 1 *E* and *E′* and Fig. S2 *E* and *E′*). The autofluorescent material colocalized in ring-like structures with the lysosomal marker Lamp1 (Fig. 1 *F* and *F′*). In the course of the disease, considerable loss of Purkinje cells was observed, becoming clearly evident at >10 mo (Fig. 1 *G* and *G′*). Neuronal cell death was accompanied by strong microgliosis (Fig. 1 *H–I′*) and astrogliosis in the cerebellar cortex (Fig. 1 *J* and *J′*).

Author contributions: M.D., I.K., M.-A.F., T.L., R.L.-R., R.D., J.D.E., and T.D. designed research; B.K., W.C.L., R.L., M.D., S.S., M.P., and R.L.-R. performed research; B.K., W.C.L., R.L., M.D., S.S., M.P., and R.L.-R. analyzed data; and M.D., T.L., R.D., J.D.E., and T.D. wrote the paper.

The authors declare no conflict of interest.

This article is a PNAS Direct Submission.

[1]W.C.L., R.L., and M.D. contributed equally to this work.

[2]To whom correspondence should be addressed. E-mail: thomas.dierks@uni-bielefeld.de.

This article contains supporting information online at www.pnas.org/lookup/suppl/doi:10.1073/pnas.1202071109/-/DCSupplemental.

www.pnas.org/cgi/doi/10.1073/pnas.1202071109

Downloaded at Palestinian Territory, occupied on December 9, 2021

www.manaraa.com

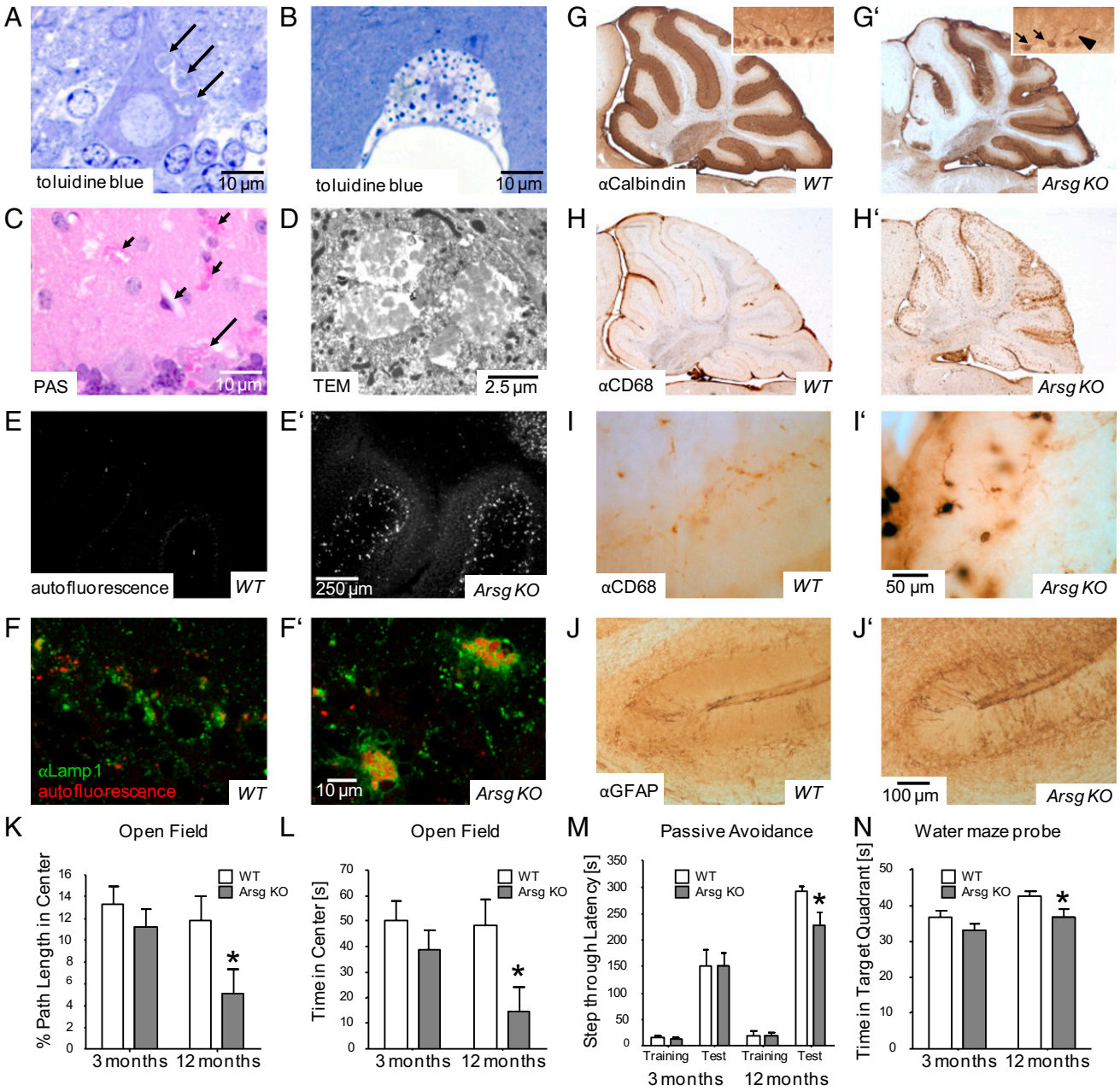

Fig. 1. Neuropathology of *Arsg*-deficient mice. (*A* and *B*) Toluidine blue-stained Epon-embedded sections of the CNS reveal storage vacuoles (arrows) in Purkinje cells (*A*) and perivascular macrophages (*B*). (*C*) Storage vacuoles in both Purkinje cells (long arrow) and macrophages (short arrows) show positive periodic acid–Schiff (PAS) staining. (*D*) TEM reveals heterogeneous, partially water-soluble, and finely granular to lamellar storage material with variable electron density in Purkinje cells. (*E* and *E′*) Fluorescence microscopy of unstained sections shows autofluorescence in the cerebellar cortex of *Arsg*-deficient mice but not in WT animals. (*F* and *F′*) Autofluorescent storage material (red) colocalizes with ring-like structures of the lysosomal membrane protein Lamp1 (green), indicating its lysosomal origin. (*G* and *G′*) Considerable loss of Purkinje cells can be observed by 12 mo of age in *Arsg*-deficient mice as assessed by Calbindin immunohistochemistry. (*Inset*) Remaining Purkinje cells show swollen dendrites (arrows) and somata (arrowhead). (*H–J′*) Profound activation of microglia transforming to an amoeboid to phagocytic morphology (*H* and *H′*, *I* and *I′*) and hypertrophy of astrocytes (*J* and *J′*) occur in *Arsg*-deficient animals in the cerebellar cortex as assessed with markers for microglia/macrophages (CD68) and astrocytes (GFAP) (age 12 mo). (*K* and *L*) *Arsg*-deficient mice showed a progressive exploratory deficit in the open-field test as indicated by reduced distance traveled (*K*) and time spent (*L*) in the center. (*M*) Lower step-through latencies indicate impaired passive-avoidance learning in *Arsg*-deficient mice. (*N*) Water-maze probe trial shows impaired visuo-spatial memory for the platform location in *Arsg*-deficient mice. For *K–N*, $n = 20$, age 12 mo; error bars indicate SEM.

Behavioral Deficits. Behavioral assays revealed that *Arsg*-knockout mice did not differ from WT littermates in grip strength, rotarod test, or treadmill performance, indicating no obvious motor abnormalities up to the age of 12 mo. However, in the open-field test, 12-mo-old *Arsg*-deficient mice traveled significantly less distance in the center of the arena ($F_{1,38} = 4.4$; $P < 0.05$) (Fig. 1*K*) and spent less time there ($F_{1,38} = 5.7$; $P < 0.05$) (Fig. 1*L*). Notably, this progressive exploratory deficit appeared not to be due to overall reduced activity because total path length and center entries revealed no significant differences among the genotypes (Fig. S3 *A* and *B*). Moreover, *Arsg*-deficient mice showed an age-dependent cognitive impairment, as could be

Downloaded at Palestinian Territory, occupied on December 9, 2021
BIOCHEMISTRY
www.manaraa.com

observed in different learning tasks. From the age of 12 mo, they displayed significantly lower step-through latencies in the testing phase of the passive-avoidance task ($F_{1,38} = 5.0$; $P < 0.05$) (Fig. 1*M*). Additionally, despite successful acquisition (Fig. S3*C*), 12-mo-old *Arsg*-deficient mice spent less time in the target quadrant during the probe trial of the water-maze task ($F_{1,38} = 4.4$; $P < 0.05$) (Fig. 1*N*). These analyses indicate that the oldest *Arsg*-deficient mice were not able to learn or to retain the spatial location of the platform as well as control mice, but were nevertheless still capable of mastering the task. Altogether, neuronal death and gliosis were accompanied by several behavioral deficits. The progressive course of these deficits with the micromorphological findings indicated manifestation of an LSD.

GAG Storage in Brain and Visceral Organs. *Arsg*-deficient mice exhibited obvious storage pathology not only in the CNS but also in several peripheral organs, including liver and kidney. Hepatocytes (Fig. 2 *A* and *A′*) and hepatic sinusoidal endothelial cells (Fig. 2 *B* and *B′*) showed accumulation of membrane-limited vacuoles filled with variable amounts of moderately or highly electron-dense and partially water-soluble material (Fig. 2 *C* and *C′*). In the kidney, the epithelia of the thick ascending limb of Henle's loop and the collecting ducts showed prominent storage (Fig. 2 *D* and *D′*). Because defects in five of the six other known lysosomal sulfatases result in lysosomal storage of undegraded GAGs (3) and become clinically evident as MPSs, we evaluated the potential of cuprolinic blue for staining of sulfated GAGs in the storage vacuoles in liver and kidney (Fig. 2 *E–F′*). Prominent cuprolinic blue staining was observed in both organs, indicating strong accumulation of GAGs. Biochemical quantification revealed a striking increase of heparan sulfate in the knockouts, ~10-fold in liver and ~3-fold in kidney and brain compared with WT (Fig. 2*G*), clearly indicating an MPS-like storage disease. Chondroitin/dermatan sulfate was low in all tissues and did not accumulate except for a twofold increase in the liver of the knockouts (Fig. 2*H*), which may reflect secondary storage induced by heparan sulfate accumulation, as reported for fibroblasts derived from MPS IIIA, IIIB, IIIC, and IIID patients (11).

Storage Material Consists of Heparan Sulfate Chains with a Terminal 3-*O*-Sulfated Glucosamine. Heparan sulfate degradation proceeds sequentially from the NRE of the chain. Thus, if ARSG is involved in heparan sulfate catabolism, the NREs of stored heparan sulfate in the knockout tissues should contain carbohydrate determinants unique to the ARSG substrate. Heparan sulfate NREs were analyzed by using an adaptation of liquid chromatography/mass spectrometry (LC/MS) (12). In this procedure, samples were depolymerized with bacterial lyases, and the products were derivatized with aniline. Heparan sulfate NREs are liberated as monosaccharides, disaccharides, and/or trisaccharides, depending on the structure of the termini (12). Analysis of heparan sulfate from *Arsg*-deficient mouse tissues revealed unique NRE structures with masses consistent with a disulfated monosaccharide (dp1) and several trisaccharides (dp3) carrying two to four sulfate groups (Fig. 3*A*). This pattern is similar but not identical to the pattern observed in heparan sulfate derived from MPS III cells and differs from the disaccharide NREs derived from other MPS disorders that affect processing of terminal uronic acids (12). This finding indicates that heparan sulfate accumulating in *Arsg*-knockout tissues most likely terminates with a glucosamine residue containing one or more sulfate groups.

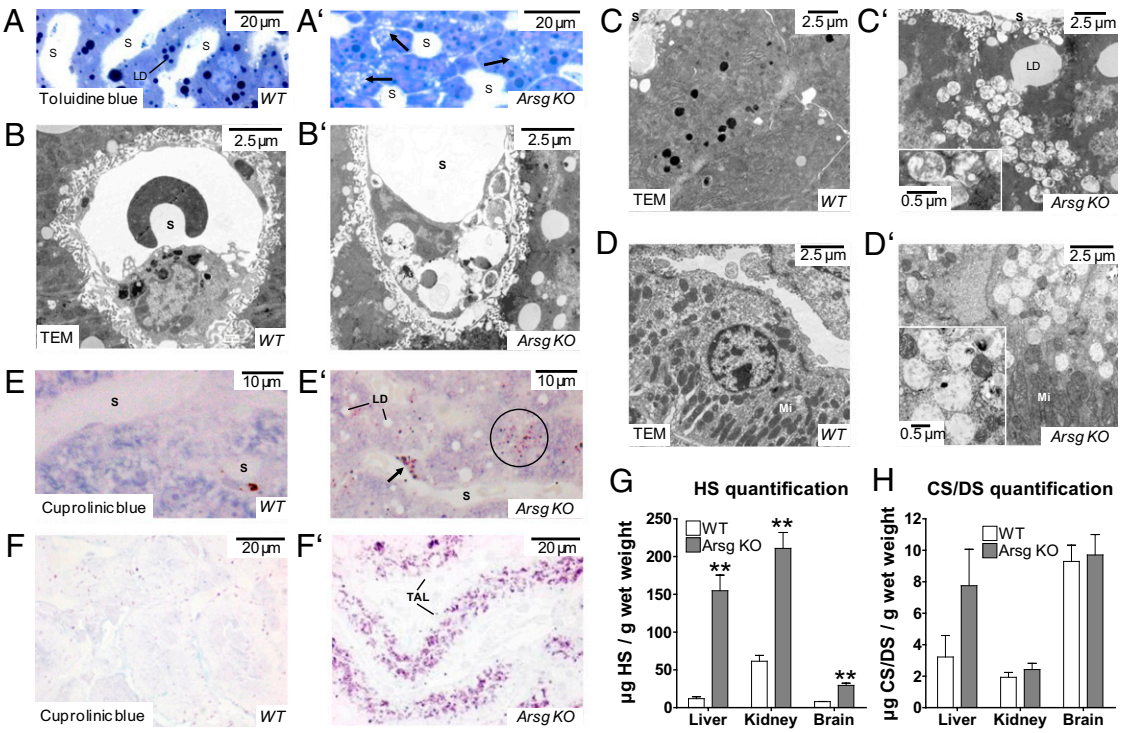

Fig. 2. Lysosomal storage pathology of liver and kidney. (*A* and *A′*) Toluidine blue-stained Epon-embedded sections of liver from *Arsg*-deficient mice (12 mo old) reveal abnormal vacuoles in the peribiliary cytoplasm of hepatocytes (arrows) (S, sinusoid; LD, lipid droplet). (*B* and *B′*) Endothelial cell of hepatic sinusoid contains cytoplasmic vacuoles with remnants of electron-dense material. (*C* and *C′*) Cytoplasmic vacuoles in hepatocytes of *Arsg*-deficient mice. (*D* and *D′*) In kidney, the epithelium of the thick ascending limbs of Henle's loop displays cytoplasmic vacuoles that appear almost empty. (*E–F′*) Cuprolinic blue incubation of liver (*E* and *E′*) and kidney (*F* and *F′*) sections reveals positive staining of inclusion bodies in hepatocytes (circle) and strong metachromatic GAG staining in liver sinusoidal cells (arrow) and in kidney thick ascending limbs (TAL) of *Arsg*-deficient mice. (*G* and *H*) Quantification of GAGs extracted from liver, brain, and kidney of *Arsg*-knockout and WT mice. The amounts of heparan sulfate (*G*) and chondroitin/dermatan sulfate (CS/DS) (*H*) were determined by LC/MS. Error bars indicate SD ($n = 3$).

Downloaded at Palestinian Territory, occupied on December 9, 2021
www.manaraa.com

Further analysis of NRE saccharides yielded the following information. First, the NRE monosaccharide comigrated with standard *N*-sulfoglucosamine-3-*O*-sulfate (GlcNS3S) (Fig. 3*B*) but not with standard *N*-sulfoglucosamine-6-*O*-sulfate (GlcNS6S) (Fig. 3*C*). Second, the mass spectrum for the NRE monosaccharide contained a single primary ion with an *m/z* value of 415, consistent with a disulfated glucosamine residue (Fig. 3*D*). Third, the storage NRE monosaccharide as well as the GlcNS3S standard did not form adduction ions with the ion-pairing agent dibutylamine (DBA) (Fig. 3*E*). In contrast, GlcNS6S yielded both primary and adduction ions (Fig. 3*F*). Fourth, tandem MS of the trisaccharide dp3(1Ac, 2S), i.e., carrying one acetyl and two sulfate groups, yielded daughter ions, confirming the presence of the disulfated glucosamine at the NRE terminus in the trisaccharide (Fig. S4*A*). This dp3 differed from a dp3 biomarker present in heparan sulfate that accumulates in MPS IIIA cells (Fig. S4*B*). Finally, treatment with propionic anhydride did not lead to a glucosamine *N*-acylation product, whereas an added unsubstituted glucosamine-containing disaccharide standard was acylated (Fig. S5). Altogether, these findings strongly suggested that the terminus consists of a 3-*O*-sulfated *N*-sulfoglucosamine (GlcNS3S) unit.

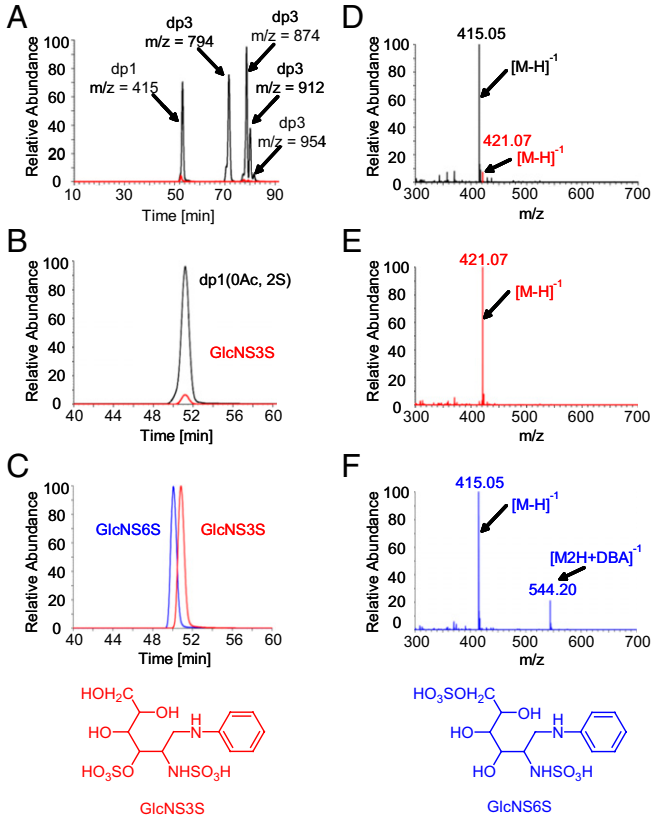

Fig. 3. NRE analysis of heparan sulfate from *Arsg*-knockout and WT livers. Heparan sulfate was enzymatically depolymerized and analyzed by LC/MS to detect the liberated NRE saccharides. (*A*) The accumulative extracted ion-current chromatograms for the indicated NRE structures are shown. One monosaccharide (dp1) and four trisaccharides (dp3) were identified as NRE saccharides in heparan sulfate from *Arsg*-knockout mouse liver (black trace). Little or no NRE structures were observed in WT liver (red trace). (*B*) Before LC/MS analysis, [$^{13}C_6$]aniline-labeled GlcNS3S (red trace) was added to depolymerized *Arsg*-knockout heparan sulfate tagged with [$^{12}C_6$]aniline (black trace). The dp1 structure shown in *A* coelutes with the standard. (*C*) An equimolar mixture of standard GlcNS3S and GlcNS6S was differentially labeled with [$^{13}C_6$]aniline and [$^{12}C_6$]aniline, respectively, and chromatographically resolved (see molecular structures after aniline labeling at the bottom of the figure). (*D*) Mass spectrum for the experiment of *B* showing both [$^{12}C_6$]aniline-labeled NRE monosaccharide (black) and [$^{13}C_6$]aniline-labeled GlcNS3S (red) with the expected 6.02 mass unit difference attributable to differential isotope labeling. (*E*) Mass spectrum for [$^{13}C_6$]aniline-labeled GlcNS3S, demonstrating only the free molecular ion (*m/z* = 421.07). (*F*) Mass spectrum for [$^{12}C_6$] aniline-labeled GlcNS6S, showing both the free molecular ion (*m/z* = 415.05, [M-H]$^-$) and a stable adduction ion (*m/z* = 544.20, [M-2H+DBA]$^-$) formed with the ion-pairing reagent DBA during LC/MS.

ARSG Acts on GlcNS3S During Heparan Sulfate Degradation. To verify that GlcNS3S is the physiological substrate of ARSG, in vitro experiments with purified recombinant human ARSG (rhARSG) were performed. rhARSG released sulfate specifically from GlcNS3S but not from the monosulfated GlcNS or glucosamine-3-sulfate (GlcN3S) (Fig. 4*A*). The recombinant human form of the closest homolog of ARSG, ARSA (rhARSA), acts on galactose 3-sulfate (4) but did not react with these substrates (Fig. 4*A*). Activity of rhARSG toward its arylsulfate pseudosubstrate *p*-nitrocatechol sulfate (pNCS) (9) was also strongly inhibited by chemically synthesized GlcNS3S (Table S1). LC/MS analysis demonstrated that rhARSG treatment of GlcNS3S, but not of GlcNS6S, resulted in nearly complete conversion to the *O*-desulfated product GlcNS (Fig. 4 *B* and *D*). No significant amount of *N*-desulfated product [GlcN3S or glucosamine-6-sulfate (GlcN6S)] was detected in any of the reactions. Finally, we demonstrated that the NRE of heparan sulfate storage material from lysosome-enriched fractions (tritosomes) isolated from *Arsg*-knockout liver is a substrate for this enzyme. Quantitative analysis by LC/MS of 250 pmol of heparan sulfate purified from *Arsg*-knockout liver yielded 18 pmol of GlcNS3S NRE monosaccharide (~1 NRE/14 disaccharides). After in vitro treatment of heparan sulfate with rhARSG, less than 1 pmol of GlcNS3S NRE was detected (Fig. 4*C*). Altogether, the data indicate that ARSG acts on terminal GlcNS3S residues in heparan sulfate to liberate the 3-*O*-sulfate group (Fig. 5).

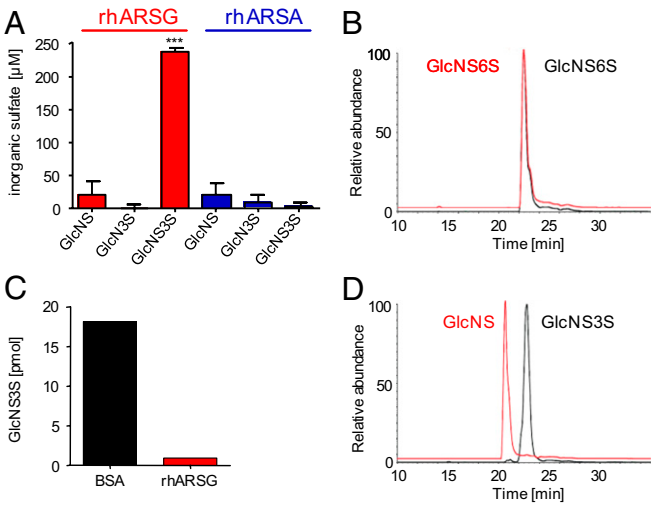

Fig. 4. In vitro analysis of ARSG substrate specificity. The activity of purified rhARSG was assayed with various substrates. (*A*) rhARSG mediates sulfate release from GlcNS3S but not from GlcNS or GlcN3S. rhARSA does not act on any of the substrates. Error bars indicate SEM (*n* = 3). (*B* and *D*) GlcNS3S, but not GlcNS6S, is desulfated to GlcNS upon treatment with ~10 mU of rhARSG for 16 h (red traces) as determined by LC/MS analysis. Controls were treated with heat-inactivated BSA (black traces). All traces represent accumulative extracted-ion-current chromatograms. (*C*) Heparan sulfate (250 pmol) from *Arsg*-knockout liver lysosome-enriched fractions (tritosomes) was subjected to quantitative NRE analysis after treatment with rhARSG (~2 mU) or heat-inactivated BSA for 16 h. The amount of GlcNS3S NRE is shown for both conditions.

Downloaded at Palestinian Territory, occupied on December 9, 2021

www.manaraa.com

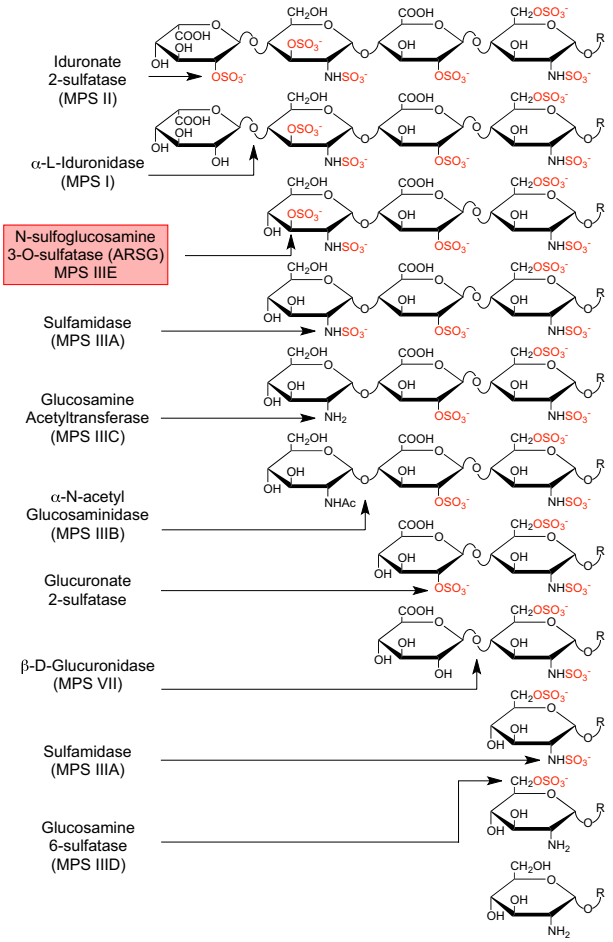

Fig. 5. Heparan sulfate catabolism involving GlcNS3S structures. The scheme illustrates all nine different enzymatic activities required for the sequential catabolism of a NRE tetrasaccharide containing GlcNS3S. To expose the 3-*O*-sulfated residue at the terminus, the preceding uronic acid (iduronate 2-*O*-sulfate in this example) is modified sequentially by iduronate 2-sulfatase and iduronidase. Under normal conditions, the 3-*O*-sulfate then is removed from GlcNS3S by ARSG, thus generating the substrate for sulfamidase, which removes the *N*-sulfate group. Subsequently, another six different enzymes (plus again sulfamidase) have to act, which ultimately leads to a complete degradation of the chain. The loss of ARSG activity (MPS IIIE) leads to the accumulation of 3-*O*-sulfated ARSG substrate that cannot be acted upon by downstream catabolic enzymes. It should be noted that the 2-*O*-sulfation shown at the glucuronic acid (third residue) is relatively rare, which agrees with the finding that no pentasulfated trisaccharides were found as NRE structures (Fig. 3*A*). Scheme modified from Neufeld and Muenzer (6) according to findings from this work and from Lawrence et al. (12).

Discussion

In this study, we demonstrate that lysosomal ARSG is a sulfatase specific for GlcNS3S residues at the NREs of heparan sulfate chains. ARSG is essential for the catabolism of heparan sulfate, as evidenced by the resulting heparan sulfate storage and MPS disease pathology in *Arsg*-deficient mice. Previous studies of *Arsg*-deficient dogs suggested that ARSG deficiency results in neuronal ceroid lipofuscinosis (NCL) (10), a type of LSD characterized by the nonspecific accumulation of autofluorescent ceroid lipopigments (13). However, we believe that classification of ARSG deficiency as a form of NCL is incorrect because ARSG behaves as a lysosomal sulfatase (9), with no apparent similarities to any of the 10 known genes associated with NCL (3, 13). Furthermore, with the exception of ARSA, which acts to degrade cerebroside 3-*O*-sulfate (sulfatide), all of the other five known lysosomal sulfatases degrade GAGs, and their deficiency causes MPS disease (3). Characterization of the NRE of stored heparan sulfate in the *Arsg*-deficient mouse, together with the demonstration that this diagnostic NRE is a specific substrate for the enzyme, now unambiguously characterizes ARSG deficiency as an MPS disorder. The accumulation of autofluorescent material, which was observed in *Arsg*-deficient dogs (10) as well as *Arsg*-deficient mice (Fig. 1 *E′* and *F′*), likely results from secondary storage, which is observed in several LSDs (14) and in MPSs in particular (15, 16).

Glucosamine residues bearing 3-*O*-sulfate groups are relatively rare in heparan sulfate and are generated by members of the 3-*O*-sulfotransferase family of enzymes (17). The rarity of this structure is likely to restrict severe storage to tissues that generate high levels of the 3-*O*-sulfated residues, which may explain why lysosomal storage in *Arsg*-knockout mice is less severe than that observed in mouse models for other MPS disorders characterized by deficiencies in enzymes that act on NRE glucosamine residues (12, 18). Interestingly, rhARSG was unable to remove the 3-*O*-sulfate group from GlcN3S, which contains a free amino group (Fig. 4*A*). There is evidence to suggest that GlcN3S can arise from the action of a subset of 3-*O*-sulfotransferases (19–21), pointing to the possibility that another 3-*O*-sulfatase may exist.

Before this study, there were four lysosomal enzymes known to be involved in processing of NRE glucosamine residues (Fig. 5): sulfamidase [MPS IIIA; Online Mendelian Inheritance in Man (OMIM) 252900]; α-*N*-acetyl-glucosaminidase (MPS IIIB; OMIM 252920); acetyl-CoA:α-glucosaminide *N*-acetyltransferase (MPS IIIC; OMIM 252930); and (*N*-acetyl)glucosamine-6-sulfatase (MPS IIID; OMIM 252940) (6), which we recently showed to act preferentially on glucosamine-6-*O*-sulfate (12). Patients lacking these enzymes have MPS type III disorders, which are subclassified as Sanfilippo diseases on the basis of their storage of heparan sulfate with a modified or unmodified glucosamine residue at the NRE as well as their pathological presentation (6). ARSG also acts on a terminal glucosamine residue, and its deficiency results in the storage of heparan sulfate, causing neuropathology and behavioral defects characteristic of other Sanfilippo disease models (18, 22–25). Thus, we propose that ARSG deficiency defines a fifth type of Sanfilippo disease, which we propose be termed MPS IIIE. Importantly, both 3-*O*-sulfotransferases and ARSG are expressed in humans (9, 17), indicating that, in addition to dogs and mice, human patients likely exist who suffer from ARSG deficiency. Hence, MPS-like patients with unclear etiology should be reanalyzed for ARSG deficiency.

In conclusion, ARSG is the missing *N*-sulfoglucosamine-3-*O*-sulfatase and shows specificity for disulfated GlcNS3S as a substrate. ARSG thus acts at a critical step in lysosomal heparan sulfate degradation and is essential for catabolism to proceed past GlcNS3S residues, which are sequentially desulfated, first by the 3-*O*-sulfatase ARSG and then by sulfamidase (Fig. 5). The knockout mouse shows that deficiency of ARSG leads to a unique, as yet unknown type of MPS, which resembles the MPS IIIA–D syndromes and hence should be termed MPS IIIE.

Materials and Methods

Targeted Disruption of Murine *Arsg*, Genotyping, and Animal Breeding. The *Arsg*-knockout mouse strain was generated by targeted disruption of the murine *Arsg* gene, and *Arsg* deficiency was validated as described in detail in Fig. S1 and in *SI Materials and Methods*. The mice were kept under standard housing conditions. All animal experiments were performed in accordance with local guidelines and were approved by local authorities.

Behavioral Analysis. Behavioral analysis was performed as described (26) with minor modifications, including neuromotor testing (rotarod, grip strength, and treadmill performance), exploratory testing (open field), and tests for learning and memory (water maze and passive avoidance).

Histological Analysis. The tissues were prepared for histochemical and immunofluorescence staining by standard procedures. Tissue samples for TEM were prepared as described previously (27). Immunohistochemistry and

Downloaded at Palestinian Territory, occupied on December 9, 2021
www.manaraa.com

immunofluorescence were performed as described elsewhere (14). Primary antibodies used were Lamp1 (Developmental Studies Hybridoma Bank), Calbindin (Sigma-Aldrich), CD68 (AbD Serotec), and GFAP (Sigma-Aldrich). Biotin-conjugated secondary antibodies were purchased from Vector Laboratories. Vectastain Elite Kit (Vector Laboratories) was used for signal amplification in immunohistochemistry, and 3,3′-diaminobenzidine tetrahydrochloride (Sigma-Aldrich) was used as substrate. Autofluorescence was detected with different wavelengths and filter settings. Cuprolinic blue staining was performed according to Scott (28). Tissue blocks were fixed in Scott's fixative containing 2.5% (vol/vol) glutaraldehyde, 0.3 M $MgCl_2$, and 25 mM sodium acetate buffer at pH 4.6. After fixation, tissue blocks were stained overnight in Scott's fixative containing 0.2% (wt/vol) cuprolinic blue dye, treated with three washes of 1% (wt/vol) Na_2WO_4 (in H_2O) and three washes of 1% (wt/vol) Na_2WO_4 [in 50% (vol/vol) ethanol], and subsequently dehydrated and processed for light microscopy (28).

Enzyme Assays. Sulfate release assays were performed with 9 mU of rhARSG or rhARSA, expressed, and purified as described (9, 29), and 500 μM GlcNS, GlcN3S (Sigma), or GlcNS3S (Dextra) in 500 mM sodium acetate (pH 5.6). Samples were incubated for 24 h at 37 °C. Released sulfate was detected and quantified by turbidimetry using a published protocol (30) with minor modifications. Briefly, a 40 mM barium chloride solution in 15% PEG 6000 was prepared. Then, 50 mL of this solution was mixed with 60 μL of a 50 mM potassium sulfate solution, and 100 μL of this mixture was added to 200 μL of the sample. After 10 min of incubation at room temperature, followed by shaking for 30 s and an additional 30-s incubation step, turbidimetry was measured at 600 nm with a TECAN Infinite M200 microplate reader.

Lysosome Isolation from Mouse Liver (Tritosomes). Lysosome-enriched fractions from mouse liver were isolated with the nonionic detergent tyloxapol (Triton WR-1339) as described previously (31).

GAG Purification. *Arsg*-knockout mice or WT animals at 12 mo of age were killed, and organs were removed and placed in ice-cold buffer [50 mM sodium acetate and 0.2 M NaCl (pH 6.0)]. After dissociation with a Polytron homogenizer, the resulting homogenates were digested on a shaker overnight at 37 °C with 0.1 mg/mL Pronase and 0.1% Triton X-100. Samples were filtered through a 0.45-μm membrane, and GAGs were purified from cell homogenates by anion-exchange chromatography as described previously (32). Briefly, 0.4 mL of diethylaminoethyl resin was washed with 20 column volumes of 50 mM sodium acetate buffer (pH 6) containing 0.2 M NaCl and 0.1% Triton X-100. After loading the samples, the column was washed with 40 column volumes of wash buffer, and GAGs were eluted with 5 column volumes of buffer containing 1 M NaCl. Samples were desalted by gel filtration (PD10), and samples were split in two for enzymatic depolymerization of heparan sulfate using 1 mU of each of heparin lyases I, II, and III or depolymerization of chondroitin/dermatan sulfate using 5 mU of chondroitinase ABC.

GAG Quantification and NRE Analysis. Depolymerized GAG preparations were derivatized by reductive amination with [$^{12}C_6$]aniline as previously described (33). Each sample was mixed with commercially available standard unsaturated monosaccharides that were tagged with [$^{13}C_6$]aniline. Samples were analyzed by LC/MS using an LTQ Orbitrap Discovery electrospray ionization mass spectrometer (Thermo Scientific) equipped with quaternary HPLC pump (Surveyor MS Pump; Finnigan) and a C-18 reverse-phase microbore column as described previously (12). DBA was used as ion-pairing reagent for LC/MS. The amount of heparan sulfate was standardized to the wet weight of processed tissue. NREs were identified on the basis of their unique mass as recently described (12).

Statistical Analysis. Results are expressed as mean ± SEM or ± SD as stated. Differences between groups were examined for statistical significance by using unpaired Student's *t* test carried out with GraphPad Prism (GraphPad Software). In figures, asterisks indicate *P* values <0.05 (*) and <0.005 (**).

ACKNOWLEDGMENTS. We thank Kerstin Böker, Christiane Grebe, Marion Knufinke, Dagmar Niemeier, and Claudia Prange for technical assistance and Kurt von Figura for critically reading the manuscript. This work was supported by Deutsche Forschungsgemeinschaft Grant DI 575/6, by funds from the Fonds der Chemischen Industrie (to T.D.), and in part by National Institutes of Health Grant R01 GM077471, a grant from the National MPS Society (to J.D.E.), and a Kirschstein National Research Service Award DK085905 (to W.C.L.).

1. Ballabio A, Gieselmann V (2009) Lysosomal disorders: From storage to cellular damage. *Biochim Biophys Acta* 1793:684–696.
2. Vitner EB, Platt FM, Futerman AH (2010) Common and uncommon pathogenic cascades in lysosomal storage diseases. *J Biol Chem* 285:20423–20427.
3. Diez-Roux G, Ballabio A (2005) Sulfatases and human disease. *Annu Rev Genomics Hum Genet* 6:355–379.
4. Mehl E, Jatzkewitz H (1968) Cerebroside 3-sulfate as a physiological substrate of arylsulfatase A. *Biochim Biophys Acta* 151:619–627.
5. von Figura K, Gieselmann V, Jaeken J (2001) Metachromatic leukodystrophy. *The Metabolic and Molecular Bases of Inherited Diseases*, eds Scriver CR, et al. (McGraw-Hill, New York), pp 3694–3724.
6. Neufeld EF, Muenzer J (2001) The mucopolysaccharidoses. *The Metabolic and Molecular Bases of Inherited Diseases*, eds Scriver CR, et al. (McGraw-Hill, New York), pp 3421–3452.
7. Shaklee PN, Glaser JH, Conrad HE (1985) A sulfatase specific for glucuronic acid 2-sulfate residues in glycosaminoglycans. *J Biol Chem* 260:9146–9149.
8. Leder IG (1980) A novel 3-*O* sulfatase from human urine acting on methyl-2-deoxy-2-sulfamino-α-D-glucopyranoside 3-sulfate. *Biochem Biophys Res Commun* 94: 1183–1189.
9. Frese M-A, Schulz S, Dierks T (2008) Arylsulfatase G, a novel lysosomal sulfatase. *J Biol Chem* 283:11388–11395.
10. Abitbol M, et al. (2010) A canine *Arylsulfatase G* (*ARSG*) mutation leading to a sulfatase deficiency is associated with neuronal ceroid lipofuscinosis. *Proc Natl Acad Sci USA* 107:14775–14780.
11. Lamanna WC, Lawrence R, Sarrazin S, Esko JD (2011) Secondary storage of dermatan sulfate in Sanfilippo disease. *J Biol Chem* 286:6955–6962.
12. Lawrence R, et al. (2012) Diagnosis and monitoring of mucopolysaccharidoses using Disease-specific non-reducing end carbohydrate biomarkers. *Nat Chem Biol* 8: 197–204.
13. Jalanko A, Braulke T (2009) Neuronal ceroid lipofuscinoses. *Biochim Biophys Acta* 1793:697–709.
14. Damme M, et al. (2011) Cerebellar alterations and gait defects as therapeutic outcome measures for enzyme replacement therapy in α-mannosidosis. *J Neuropathol Exp Neurol* 70:83–94.
15. McGlynn R, Dobrenis K, Walkley SU (2004) Differential subcellular localization of cholesterol, gangliosides, and glycosaminoglycans in murine models of mucopolysaccharide storage disorders. *J Comp Neurol* 480:415–426.
16. Wisniewski K, et al. (1985) Sanfilippo disease, type A with some features of ceroid lipofuscinosis. *Neuropediatrics* 16:98–105.
17. Esko JD, Selleck SB (2002) Order out of chaos: Assembly of ligand binding sites in heparan sulfate. *Annu Rev Biochem* 71:435–471.
18. Li HH, et al. (1999) Mouse model of Sanfilippo syndrome type B produced by targeted disruption of the gene encoding α-*N*-acetylglucosaminidase. *Proc Natl Acad Sci USA* 96:14505–14510.
19. Liu J, et al. (1999) Heparan sulfate D-glucosaminyl 3-*O*-sulfotransferase-3A sulfates *N*-unsubstituted glucosamine residues. *J Biol Chem* 274:38155–38162.
20. Liu J, et al. (2002) Characterization of a heparan sulfate octasaccharide that binds to herpes simplex virus type 1 glycoprotein D. *J Biol Chem* 277:33456–33467.
21. Vanpouille C, et al. (2007) The heparin/heparan sulfate sequence that interacts with cyclophilin B contains a 3-*O*-sulfated *N*-unsubstituted glucosamine residue. *J Biol Chem* 282:24416–24429.
22. Bhaumik M, et al. (1999) A mouse model for mucopolysaccharidosis type III A (Sanfilippo syndrome). *Glycobiology* 9:1389–1396.
23. Ohmi K, et al. (2003) Activated microglia in cortex of mouse models of mucopolysaccharidoses I and IIIB. *Proc Natl Acad Sci USA* 100:1902–1907.
24. Crawley AC, et al. (2006) Characterization of a C57BL/6 congenic mouse strain of mucopolysaccharidosis type IIIA. *Brain Res* 1104:1–17.
25. Lau AA, Crawley AC, Hopwood JJ, Hemsley KM (2008) Open field locomotor activity and anxiety-related behaviors in mucopolysaccharidosis type IIIA mice. *Behav Brain Res* 191:130–136.
26. D'Hooge R, et al. (2005) Neurocognitive and psychotiform behavioral alterations and enhanced hippocampal long-term potentiation in transgenic mice displaying neuropathological features of human α-mannosidosis. *J Neurosci* 25:6539–6549.
27. Kollmann K, et al. (2009) Molecular characterization and gene disruption of mouse lysosomal putative serine carboxypeptidase 1. *FEBS J* 276:1356–1369.
28. Scott JE (1980) Collagen–proteoglycan interactions. Localization of proteoglycans in tendon by electron microscopy. *Biochem J* 187:887–891.
29. Dierks T, Schmidt B, von Figura K (1997) Conversion of cysteine to formylglycine: A protein modification in the endoplasmic reticulum. *Proc Natl Acad Sci USA* 94: 11963–11968.
30. Lundquist P, Mårtensson J, Sörbo B, Ohman S (1980) Turbidimetry of inorganic sulfate, ester sulfate, and total sulfur in urine. *Clin Chem* 26:1178–1181.
31. Wattiaux R, Wibo M, Baudhuin P (1963) Effect of the injection of Triton WR 1339 on the hepatic lysosomes of the rat (Translated from French). *Arch Int Physiol Biochim* 71: 140–142.
32. Esko JD (2001) Special considerations for proteoglycans and glycosaminoglycans and their purification. *Curr Protoc Mol Biol* 22:17.2.1–17.2.9.
33. Lawrence R, et al. (2008) Evolutionary differences in glycosaminoglycan fine structure detected by quantitative glycan reductive isotope labeling. *J Biol Chem* 283: 33674–33684.

BIOCHEMISTRY
Downloaded at Palestinian Territory, occupied on December 9, 2021
www.manaraa.com